Int. J. Environ. Sci. Technol. (2012) 9:463–472
DOI 10.1007/s13762-012-0043-9

ORIGINAL PAPER

Adsorption of chromium (VI) from aqueous solution by the iron (III)-impregnated sorbent prepared from sugarcane bagasse

Y. Zhu · H. Zhang · H. Zeng · M. Liang · R. Lu

Received: 6 December 2010 / Revised: 25 August 2011 / Accepted: 24 October 2011 / Published online: 20 March 2012

Abstract An iron (III)-impregnated sorbent was prepared from sugarcane bagasse and ferric chloride solution via carbonization/activation in a muffle furnace at 500 °C for 4 h. The adsorption removal of chromium (VI) from aqueous solution by the iron (III)-impregnated sorbent was then studied in a batch system. With increasing initial chromium (VI) concentration from 25 to 130 mg/L at an adsorbent dose of 300 mg/50 mL, the amount of adsorbed chromium (VI) increased from 4.15 to 12.20 mg/g at 20 °C, from 4.16 to 12.50 mg/g at 30 °C, and from 4.16 to 13.72 mg/g at 40 °C. The dynamical data fit very well with the pseudo-second-order kinetic model, and the calculated adsorption capacities of 4.16, 8.37, and 13.37 mg/g were equal to the actual values of the experiments at the initial chromium (VI) concentrations of 25, 50, and 100 mg/L, respectively. The Langmuir isotherm could yield better fits than the Freundlich isotherm. The calculated isotherm parameters confirmed the favorable adsorption of chromium (VI) on the iron (III)-impregnated sorbent.

Keywords Adsorption removal · Agricultural waste · Hematite · Hexavalent chromium · Isotherm · Kinetic model

Introduction

Hexavalent chromium (chromium(VI), Cr(VI)) is a well-known highly toxic metal, considered a priority pollutant. The presence of high levels of chromium in the environment may cause long-term health risks to humans and ecosystems (Mohan and Pittman 2006; Gupta and Babu 2009; Witek-Krowiak et al. 2010). Industrial sources of Cr(VI) include leather tanning, cooling tower blowdown, plating, electroplating, anodizing baths, rinse waters, etc. (Mohan and Pittman 2006). Its removal from industrial wastewater prior to discharge into environment is, therefore, necessary to avoid long-term health risks. The maximum contaminant level goal of chromium for the drinking water is 0.05 mg/L for the World Health Organization set standard (Witek-Krowiak et al. 2010). The drinking water guideline recommended by the Environmental Protection Agency of United States of America is 0.10 mg/L (Mohan and Pittman 2006).

Contaminants from industrial wastewater rich in chromium, lead, cadmium, and other heavy metal ions remain an important environmental issue (Abdel-Ghani et al. 2009; Okoye et al. 2010; Rafati et al. 2010). Although control technologies have been applied to many industrial and municipal wastewater sources, the total quantity of these agents released to the environment remains staggering (Mohan and Pittman 2006). A wide range of treatment technologies, such as chemical precipitation, ion-exchange, membrane separation, electrocoagulation, solvent extraction, reduction, reverse osmosis and adsorption, have been developed to remove chromium from water and wastewater. Most of them are very effective at removing chromium from water and wastewater containing relatively high initial chromium concentrations (Chu and Hashim 2002; Gupta and Babu 2009). Adsorption is generally known to be one of the most effective techniques for chromium removal and recovery from aqueous wastes (Bayrak et al. 2006; Gupta and Babu 2009; Samani et al. 2010; Witek-Krowiak et al. 2010). Selective adsorption by biological materials, mineral oxides, activated carbons, or polymer resins has generated

---

Y. Zhu (✉) · H. Zeng · M. Liang · R. Lu
College of Environmental Science and Engineering,
Guilin University of Technology, Guilin 541004, P. R. China
e-mail: zhuyinian@glite.edu.cn

H. Zhang
Institute of Light Industry and Food Engineering,
Guangxi University, Nanning 530004, P. R. China

increasing excitement. In general, activated carbons are widely applied effective adsorbents for wastewater treatment and have been studied extensively (Chu and Hashim 2002; Mohan and Pittman 2006; Bayrak et al. 2006).

Considerable attention has been paid to the development of effective and low-cost adsorbents and to evaluate their capacity for chromium removal (Chu and Hashim 2002; Mohan and Pittman 2006; Gupta and Babu 2009). If inexpensively alternative adsorbents can be developed, it would be beneficial to the environment and have attractive commercial value. In this respect, various materials, such as agricultural wastes, industrial waste/by-products, zeolite, organic resins, synthesized fibers, carbon steel, lignite, peat, chars, coals, clay minerals, and oxides/hydroxides have been investigated for chromium adsorption (Crini 2005; Mohan and Pittman 2006).

Activated carbon is a black solid substance resembling granular or powder charcoal, and is widely used as adsorbents in wastewater and gas treatments (Baçaoui et al. 2001; Sahu et al. 2010). Despite its prolific use in environmental protection, activated carbon remains an expensive material. In the recent years, research interest in the production of low-cost alternatives to activated carbon has grown (Khalili et al. 2000). Agricultural wastes have emerged as a better choice for preparing activated carbons (Witek-Krowiak et al. 2010). Though raw agricultural wastes can be used as adsorbents without further treatment, activation could enhance their adsorption capacity. The production of activated carbons from agricultural wastes convert unwanted, surplus agricultural waste, of which billions of kilograms are produced annually, to useful valuable adsorbents (Mohan and Singh 2002; Sahu et al. 2010).

Sugarcane bagasse is the fibrous waste left after the extraction of sugar juice from crushed cane. Sugarcane refining generates a large volume of residue called bagasse. Sugarcane bagasse in its natural state is a poor adsorbent of organic compound such as sugar colorants and metal ions (Qureshi et al. 2008; Boussarsar et al. 2009). Since bagasse is a highly carbonaceous agricultural byproduct, a natural outlet would be to use bagasse as a feedstock in the manufacture of activated carbons, which can then be used in the wastewater treatment process. Bagasse is reported as a suitable resource for the preparation of activated carbon (Ioannidou and Zabaniotou 2007; Wong et al. 2009; Brandão et al. 2010).

In the present work, a ferric iron (Fe(III))-impregnated sorbent was prepared from sugarcane bagasse and ferric chloride ($FeCl_3$) and then was used to investigate the adsorption of Cr(VI) from aqueous solution. Studies concerning the effects of contact time, temperature, adsorbent dose, initial phosphorus concentration, and negative decimal logarithm of the hydrogen ion activity (pH) are presented and discussed. Experimental data were analyzed using kinetic equations and equilibrium isotherms. The characteristic parameters for each model have been determined. This research has been carried out in the Guangxi Key Laboratory of Environmental Engineering, Protection and Assessment, P. R. China, from July 2009 to January 2011.

Materials and methods

Preparation and characterization of the Fe(III)-impregnated sorbent

Sugarcane bagasse was collected from a sugar industry, Guangxi, China. The reagents ferric chloride hexahydrate ($FeCl_3 \cdot 6H_2O$) and cetyl-trimethyl ammonium bromide (CTMAB) were bought from Country Medicine Group, Shanghai, China. The bagasse was left to dry in oven at 80 °C for 24 h; then, it was cut into small pieces and sieved to an average particle size of 5 mm. 1 mol/L $FeCl_3$ solution, 0.05 mol/L CTMAB solution, 1 and 10 % (v/v) ammonia solutions were prepared from chemical reagents of analytical grade and ultrapure water.

800 mL ultrapure water and 100 mL of 0.05 mol/L CTMAB solutions were added into a 2-L beaker and heated to boiling. Then, 100 mL of 1 mol/L $FeCl_3$ solution was added into the beaker slowly under stirring to obtain a red-brown colloid solution. 50 g dried bagasse was added to the colloid solution and mixed. After soaking for 24 h, the mixture of the colloid solution and bagasse was adjusted to $pH = 7.4$ with 10 % (v/v) ammonia solution using the automatic potentiometric titrator (Metrohm 848 Titrino Plus). Under this condition, a bagasse–ferric hydroxide ($Fe(OH)_3$) mixture was formed in the suspended solution. The suspended solid was filtered and dried in oven at 105–110 °C for 24 h. Finally, the bagasse-$Fe(OH)_3$ solid was carbonized/activated in a muffle furnace at 500 °C for 4 h to get the Fe(III)-impregnated sorbent. The sample was ground and sifted to obtain a powder with a particle size smaller than 0.124 mm (120 mesh).

The specific surface area of the Fe(III)-impregnated sorbent was determined from nitrogen adsorption/desorption isotherms measured at -194 °C (boiling point of nitrogen gas at atmospheric pressure) by a Quantachrome NOVAe1000. Prior to gas adsorption measurements, the activated carbon was degassed at 200 °C in a vacuum condition for a period of at least 4 h. The surface area was determined by the Brunauer–Emmet–Teller (BET) method. The total pore volume (V_{total}) and the average pore diameter (d_{av}) were derived from the Barrett–Joyner–Halenda (BJH) method. BET surface area and the BJH desorption surface area of the Fe(III)-impregnated sorbent were determined to be 26.79 and 32.58 m^2/g, respectively. The total pore volume and the average pore diameter were derived from the BJH method to be 0.0201 cm^3/g and 12.25 nm, respectively.

The prepared Fe(III)-impregnated sorbent was characterized by powder X-ray diffraction (XRD) with a X'Pert PRO diffractometer using Cu Kα radiation (40 kV and 40 mA). Crystallographic identification of the prepared sorbent was accomplished by comparing the experimental XRD pattern to that of the International Center for Diffraction Data (ICDD), standard hematite (α-Fe_2O_3) (00-033-0664). The XRD result showed the crystalline structure of the sugarcane bagasse and the Fe(III)-impregnated sorbent. All the major peaks in the pattern from the prepared Fe(III)-impregnated sorbent could be clearly seen and identified as belonging to standard hematite (α-Fe_2O_3). This confirms the formation of hematite (α-Fe_2O_3) during the sorbent preparation.

The morphology was analyzed by scanning electron microscopy (SEM, Joel JSM-6380LV). The SEM images indicated that the particle sizes of activated carbons and hematite (α-Fe_2O_3) in the Fe(III)-impregnated sorbent were 400 nm–1 μm and <500 nm, respectively.

Adsorption experiments

Effects of adsorption conditions

The experiments were carried out in a set of plastic centrifuge tubes (100 mL) by agitating desired amounts of the Fe(III)-impregnated sorbent powder in 50 mL Cr(VI) solutions of desired concentration and pH with an isothermal shaker (20, 30, or 40 °C) at the agitation speed of 200 rpm to reach equilibrium of the solid-solution mixture. After centrifuged at 4,000 rpm for 5 min, all samples were filtered through 0.45-μm micro-pore membrane, and aqueous Cr(VI) concentrations were determined by the 1,5-diphenylcarbohydrazide spectrophotometric method measuring the absorbance at 540 nm by using a spectrophotometer (Lambda 25 UV/VIS, Perkin Elmer).

Effect of pH was studied by adjusting the initial pH of Cr(VI) solutions using diluted hydrochloric acid (HCl) and sodium hydroxide (NaOH) solutions (pHs 1, 2, 3, 4, 5, 6, 7, 8, 9, and 10), and the solutions were agitated with 0.3 g/50 mL adsorbent dose for 50 mg/L Cr(VI) concentrations at 30 °C. Eleven initial Cr(VI) concentrations (25, 40, 50, 60, 70, 80, 90, 100, 110, 120, and 130 mg/L) were employed for the study of initial concentration effect on adsorption at 20, 30, or 40 °C. Effect of adsorbent dosage was studied with different adsorbent doses (0.1, 0.2, 0.3, 0.4, 0.5, and 0.6 g) and 50 mL of 50 mg/L Cr(VI) solutions with initial pH 5 at 30 °C.

Adsorption kinetics

Kinetic studies were carried out in a set of plastic centrifuge tubes (100 mL) at constant temperatures (20, 30, or 40 °C), by shaking 0.3 g of the Fe(III)-impregnated sorbent powder in 50 mL Cr(VI) solutions (25, 50, or 100 mg/L) in each capped plastic centrifuge tube at the stirring speed of 200 rpm. The aqueous samples were taken from different conical flasks at different time intervals of 0.25, 0.5, 1, 1.5, 2, 3, 6, 9, 12, 15, 18, 24, 30, 36, 42, 48, 54, 60, 72, and 84 h, respectively. All the samples were centrifuged and filtered similarly through a 0.45-μm membrane filter in order to remove the carbon fines, and then, the total Cr(VI) concentrations in aqueous solutions were determined by the 1,5-diphenylcarbohydrazide spectrophotometric method, measuring the absorbance at 540 nm by using a spectrophotometer (Lambda 25 UV/VIS, Perkin Elmer). The amount of adsorption at time t, q_t (mg/g), was calculated as follows: $q_t = (C_0 - C_t)V/W$, where C_0 and C_t (mg/L) are the liquid-phase concentrations of Cr(VI) at initial and at any time t, respectively. V is the volume of the solution (L), and W is the mass of the prepared activated carbon used (g).

Adsorption isotherm

Adsorption isotherms were performed in a set of plastic centrifuge tubes (100 mL), where solutions of Cr(VI) (50 mL) with different initial concentrations (25, 40, 50, 60, 70, 80, 90, 100, 110, 120, and 130 mg/L) were placed. Equal masses of 0.3 g of the Fe(III)-impregnated sorbent powder were added to Cr(VI) solutions, and each sample was kept in an isothermal shaker (20, 30, or 40 °C) at a stirring speed of 200 rpm for 72 h to reach equilibrium of the solid-solution mixture. The tubes were then removed from the shaker, and the final concentration of Cr(VI) in the solution was analyzed. The amount of adsorption at equilibrium, q_e (mg/g), was calculated as follows: $q_e = (C_0 - C_e)V/W$, where C_0 and C_e (mg/L) are the liquid-phase concentrations of Cr(VI) at initial and equilibrium, respectively. V is the volume of the solution (L), and W is the mass of the prepared activated carbon used (g).

Results and discussions

Effects of adsorption conditions

Adsorption equilibrium is governed by several operational factors, such as the nature of solute and adsorbent as well as the pH of the medium. In this study, the effect of the contact time, temperature, the solution pH, the mass of the prepared Fe(III)-impregnated sorbent, and the initial concentration on adsorption kinetics was investigated.

Contact time

The adsorption rate denoted by dq/dt shows how much adsorbate can be adsorbed from the liquid phase onto the adsorbent within a unit of time. In a diagram depicting the q_t–t relationship, the slope at each point of the curve represents the instantaneous adsorption rate dq/dt (Yang and Al-Duri 2005). The effect of the contact time on the adsorption kinetics is shown in Fig. 1 in terms of the q_t–t relationship. The Cr(VI) concentration decreased rapidly with the contact time and this confirmed strong interactions between the Cr(VI) and the adsorbent. In other words, the adsorption capacity increased with contact time. Figure 1 reveals that the amount of Cr(VI) adsorbed (mg/g) increased with the contact time until it gradually approaches the equilibrium state due to the continuous decrease in the driving force ($q_e - q_t$). The amount of Cr(VI) adsorbed and the concentration of Cr(VI) in the liquid phase remained almost constant, after adsorption for 360, 2,880, 4,320 min at 30 °C and pH 5 with the initial Cr(VI) concentration of 25, 50, and 100 mg/L, respectively.

It is also observed that for an initial Cr(VI) concentration of 25 mg/L at 20 °C and pH 5, the maximum amount of Cr(VI) was adsorbed within the first 360 min at an average adsorption rate of 0.0116 mg/(g min) (99.95 % of total amount of Cr(VI) adsorbed). A similar trend was observed for the initial Cr(VI) concentrations of 50 and 100 mg/L. The contact time between adsorbate and the adsorbent is of significant importance in adsorption. In physical adsorption, most of the adsorbate species are adsorbed within a short interval of contact time. However, strong chemical binding of the adsorbate with adsorbent requires a longer contact time for the attainment of equilibrium. Available adsorption studies in literature reveal also that the uptake of adsorbate species is fast at the initial stages of the contact period, and, thereafter, it becomes slower near the equilibrium (Doğan et al. 2007). The initial rapid uptake of adsorbate species may be due to large numbers of available vacant sites on the adsorbent surface at the initial stage (Kavitha and Namasivayam 2007).

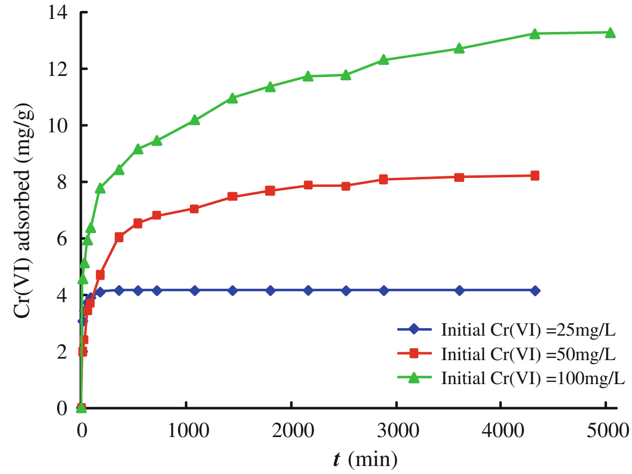

Fig. 1 Effect of contact time on Cr(VI) adsorption onto the Fe(III)-impregnated sorbent

Adsorbent dose

The adsorption of Cr(VI) onto the Fe(III)-impregnated sorbent was studied by varying the adsorbent quantity in the test solution while keeping the initial Cr(VI) concentration, initial pH, and contact time constant at 30 °C (Fig. 2). Increase in adsorption with adsorbent dose can be attributed to increased adsorbent surface area and availability of more adsorption sites, but unit adsorption decreased with increase in the adsorbent dose. This may be attributed to overlapping or aggregation of adsorbent surface area available to Cr(VI), and an increase in diffusion path length. The amount of Cr(VI) adsorbed per unit mass of adsorbent decreased with increasing adsorbent quantity in test solution from 11.19 to 4.16 mg/g. On the contrary, the percentage of Cr(VI) removed from solution increased continuously from 44.85 to 99.78 % with increasing adsorbent dosages from 100 to 600 mg in 50 mL test solution. Similar to the amount of Cr(VI) adsorbed, the solution pH at equilibrium decreased from 2.79 to 2.07 with increasing adsorbent quantity from 0.1 to 0.6 g in test solution.

Initial concentration and temperature

The kinetic dependencies were also measured for various initial Cr(VI) concentrations (25–130 mg/L) at 20, 30, and 40 °C, whereas the other experimental parameters were kept constant. The dependencies of the amount of Cr(VI) adsorbed, q_e, and the removal percentage versus the initial concentration are shown in Fig. 3. The overall trend for different temperatures was similar, i.e., with increasing Cr(VI) concentrations in test solution from 25 to 130 mg/L, the actual amount of Cr(VI) adsorbed per unit mass of adsorbent increased from 4.15 to 12.20 mg/g at 20 °C, from 4.16 to

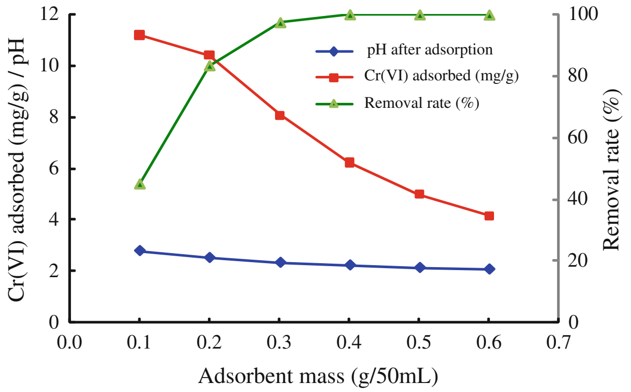

Fig. 2 Effect of adsorbent dose on Cr(VI) adsorption onto the Fe(III)-impregnated sorbent

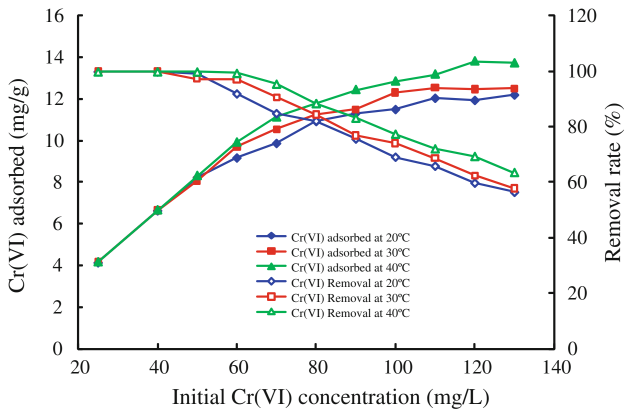

Fig. 3 Effect of initial concentration and temperature on Cr(VI) adsorption onto the Fe(III)-impregnated sorbent

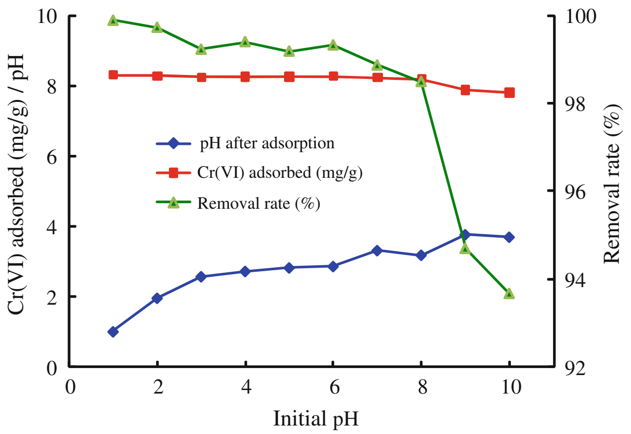

Fig. 4 Effect of initial pH on Cr(VI) adsorption onto the Fe(III)-impregnated sorbent

12.50 mg/g at 30 °C and from 4.16 to 13.72 mg/g at 40 °C, which confirmed strong physical and chemical interactions between Cr(VI) and the Fe(III)-impregnated sorbent. When the initial Cr(VI) concentration was higher than 100 mg/L, the unit adsorption for Cr(VI) remained almost constant and did not increase obviously with initial Cr(VI) concentration. If the results are expressed in percentage of Cr(VI) removed from solution, the percent adsorption decreased continuously from 99.85 to 56.44 % at 20 °C, 99.86 to 57.86 % at 30 °C, and 99.84 to 63.46 % at 40 °C, with increase in initial Cr(VI) concentration from 25 to 130 mg/L.

As also shown in Fig. 3, the adsorption capacity increased with the increase in adsorption temperature; therefore, the Cr(VI) adsorption was an endothermic reaction in this study. Increasing the temperature is known to increase the rate of diffusion of the adsorbate molecules across the external boundary layer and in the internal pores of the adsorbent particles, owing to the decrease in the viscosity of the solution. In addition, changing temperature will change the equilibrium capacity of the adsorbent for a particular adsorbate (Doğan et al. 2007).

Solution pH

The pH of the solution plays an important role in the whole adsorption process, influencing not only the solution Cr(VI) chemistry, but also the surface charge of the adsorbent (Crini 2008). Effect of initial solution pH on the adsorption of Cr(VI) is shown in Fig. 4. Cr(VI) upon dissolution formed Cr(VI) anions in solution. The adsorption of these charged Cr(VI) groups onto the adsorbent surface was primarily influenced by the surface charge on the adsorbent which, in turn, was influenced by pH of the solution (Crini 2008). After adsorption, the solution pH decreased under both acidic and basic conditions. Low initial pH favored the adsorption of Cr(VI) onto the Fe(III)-impregnated sorbent. As the initial pH increased from 1 to 10, the adsorption capacity decreased from 8.31 to 7.80 mg/g, and the corresponding removal rate decreased from 99.89 to 93.68 %. Especially when the initial pH was greater than 8, the adsorption capacity and the corresponding removal rate decreased drastically.

Adsorption kinetics

The study of adsorption equilibrium and kinetics is essential in supplying the fundamental information required for the design and operation of adsorption equipments for wastewater treatment. In order to investigate the mechanism of adsorption, this paper employs the four different kinetic models, namely the pseudo-first-order equation, the modified pseudo-first-order equation, the pseudo-second-order equation, and the intraparticle diffusion model.

Pseudo-first-order kinetic model

The equation corresponding to the pseudo-first-order kinetic model is the following differential form (Okoye et al. 2010):

$$\frac{\mathrm{d}q_t}{\mathrm{d}t} = k_1(q_\mathrm{e} - q_t) \tag{1}$$

Integrating this for the boundary condition $q_\mathrm{e} = 0$ at $t = 0$ and $q_t = q_t$ at $t = t$, gives:

$$\ln\frac{q_\mathrm{e}}{q_\mathrm{e} - q_t} = k_1 t \tag{2}$$

where q_e and q_t refer to the amount of Cr(VI) adsorbed (mg/g) at equilibrium and at any time, t (min), respectively, and k_1 is the equilibrium rate constant of the pseudo-first-order sorption (min^{-1}). Equation (2) can be rearranged to obtain a linear form:

$$\ln(q_\mathrm{e} - q_t) = \ln q_\mathrm{e} - k_1 t \tag{3}$$

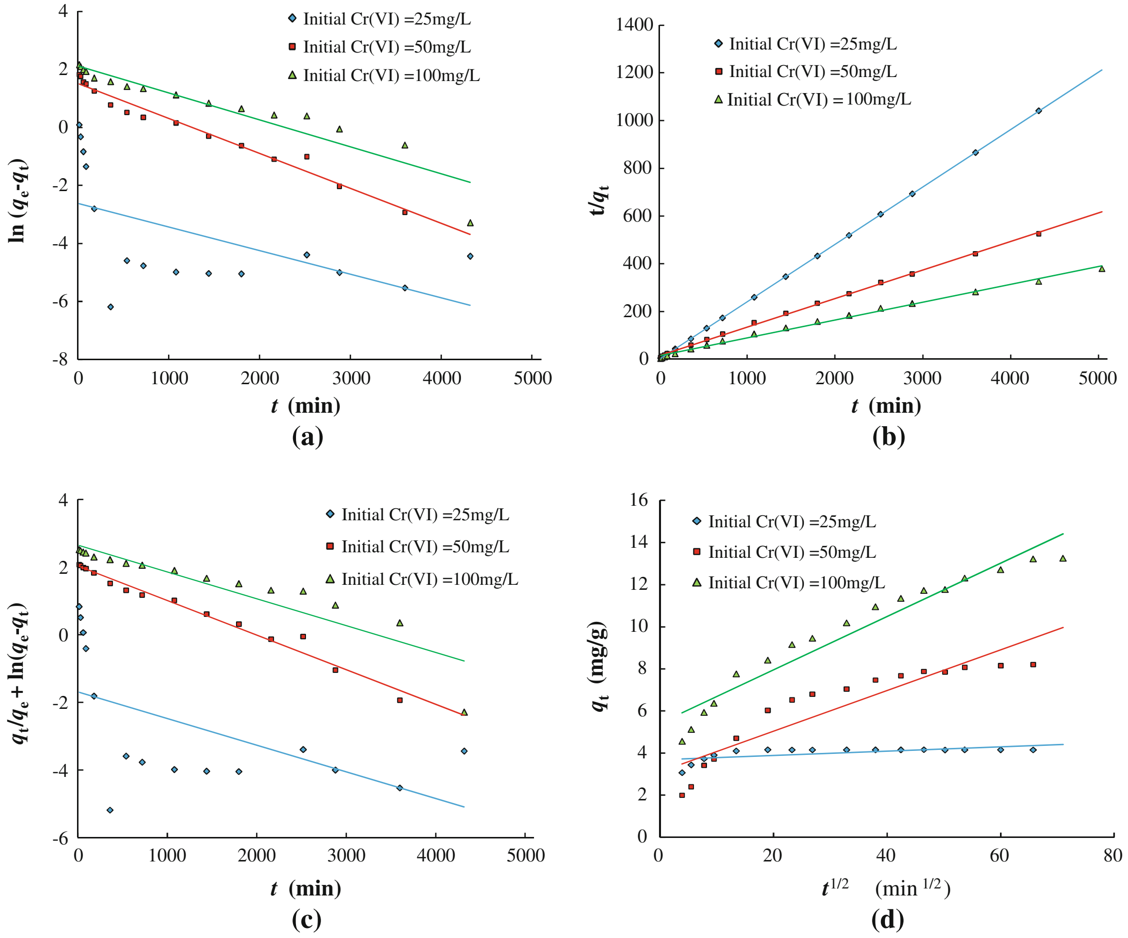

Fig. 5 Four kinetic models for Cr(VI) adsorption onto the Fe(III)-impregnated sorbent. **a** Pseudo-first-order kinetic model, **b** modified pseudo-first-order kinetic model, **c** pseudo-second-order kinetic model, **d** intraparticle diffusion kinetic model

The plot of $\ln(q_e - q_t)$ against t should give a straight line with slope $-k_1$ and intercept $\ln q_e$ (Fig. 5). The values of k_1 and q_e at different initial Cr(VI) concentrations are presented in Table 1. As seen in Table 1, the correlation coefficient value R^2 for Cr(VI) adsorption onto the Fe(III)-impregnated sorbent changed in the range of $0.3119 - 0.9721$. These results have shown that the experimental data do not well agree with the pseudo-first-order kinetic model.

Modified pseudo-first-order kinetic model

The pseudo-first-order equation represented by Eq. (1) is modified through the modification of its rate constant (Yang and Al-Duri 2005). Denoting the rate constant in the modified pseudo-first-order rate equation by K_1 (min^{-1}), the following equation is proposed:

$$k_1 = K_1 \frac{q_e}{q_t} \tag{4}$$

As $q_t < q_e$, the above equation implies that the rate constant k_1 is minimum when equilibrium is reached.

The modified pseudo-first-order rate equation can be derived as follows:

$$\frac{dq_t}{dt} = K_1 \frac{q_e}{q_t}(q_e - q_t) \tag{5}$$

Equation (5) can be rearranged into

$$-dq_t + \frac{q_e dq_t}{(q_e - q_t)} = K_1 q_e dt \tag{6}$$

Integrating Eq. (6) over time from 0 to t, while the solid phase concentration increases from 0 to q_t, the following algebraic equation can be obtained:

$$\frac{q_t}{q_e} + \ln(q_e - q_t) = \ln(q_e) - K_1 t \tag{7}$$

If the adsorption process follows the modified pseudo-first-order kinetic model represented by Eq. (7), a plot of $q_t/q_e + \ln(q_e - q_t)$ against t should be a straight line (Fig. 5). The values of K_1 and q_e at different temperatures are presented in Table 1. As seen in Table 1, the correlation

Table 1 Kinetic and isotherm parameters for Cr(VI) adsorption onto the Fe(III)-impregnated sorbent

Pseudo-first-order constants

Initial Cr(VI) concentration (mg/L)	k_1/(1/min)	q_e (mg/g)	R^2
25	0.0008	0.0733	0.3119
50	0.0012	4.5581	0.9721
100	0.0009	8.3578	0.8835

Modified pseudo-first-order constants

Initial Cr(VI) concentration (mg/L)	K_1/(1/min)	q_e (mg/g)	R^2
25	0.0008	0.184	0.3117
50	0.0010	7.633	0.9788
100	0.0008	14.129	0.8304

Pseudo-second-order constants

Initial Cr(VI) concentration (mg/L)	k_2/(g/(mg min))	q_e (mg/g)	h/(g/(mg min))	R^2
25	0.000261	4.16	1.4027	1.0000
50	0.000070	8.37	0.0652	0.9990
100	0.000032	13.37	0.0691	0.9946

Intraparticle diffusion constants (fitting data with single straight line)

Initial Cr(VI) concentration (mg/L)	K_d/(mg/(g min$^{1/2}$))	R^2
25	0.0103	0.4281
50	0.0966	0.8368
100	0.1265	0.9399

Langmuir constants

Temperature (°C)	q_m (mg/g)	K_L (L/mg)	R_L	R^2
20	12.22	0.9435	0.0081–0.0407	0.9981
30	12.63	1.3222	0.0058–0.0294	0.9990
40	13.72	1.6720	0.0046–0.0234	0.9982

Freundlich constants

Temperature (°C)	K_F (mg$^{1-1/n}$L$^{1/n}$g^{-1})	$1/n$	R^2
20	7.742	0.1194	0.8993
30	8.022	0.1258	0.9062
40	9.077	0.1194	0.8203

coefficient values for Cr(VI) adsorption onto the Fe(III)-impregnated sorbent changed in the range of 0.3117 − 0.9788. This result has shown that the experimental data did not fit well with the modified pseudo-first-order kinetic model.

Pseudo-second-order kinetic model

The equation corresponding to the pseudo-second-order kinetic model is the following (McKay and Ho 1999):

$$\frac{dq_t}{dt} = k_2(q_e - q_t)^2 \tag{8}$$

Integrating this for the boundary condition $t = 0$, $q_e = 0$, $t = t$, $q_t = q_t$ gives:

$$\frac{1}{q_e - q_t} = \frac{1}{q_e} + k_2 t \tag{9}$$

where k_2 is the equilibrium rate constant of the pseudo-second-order adsorption (g/(mg min)). Eq. (9) can be arranged to obtain a linear form:

$$\frac{t}{q_t} = \frac{1}{k_2 q_e^2} + \frac{1}{q_e} t \tag{10}$$

the initial adsorption rate, h (mg/(g min)), as $t = 0$ can be defined (Kavitha and Namasivayam 2007):

$$h = k_2 q_e^2 \tag{11}$$

where the initial adsorption rate (h), the equilibrium adsorption capacity (q_e), and the second-order constants k_2 (g/(mg min)) can be determined experimentally from the slope and intercept of plot t/q_t versus t (Fig. 5). Calculated correlations are closer to unity for second-order kinetics model ($R^2 = 0.9946 - 1.0000$); therefore, the adsorption kinetics could well be approximated more favorably by second-order kinetic model for Cr(VI) adsorption onto the Fe(III)-impregnated sorbent. The k_2 and h values are calculated from Fig. 5 to be 0.000032 − 0.000261 g/(mg min) and 0.0652 − 1.4027 mg/(g min), respectively (Table 1). The equilibrium adsorption capacities (q_e) were equal to the actual values that were be determined by the experiment.

Intraparticle diffusion kinetic model

The Cr(VI) sorption is governed usually by either the liquid phase mass transport rate or the intraparticle mass transport rate. Intraparticle diffusion model assumes that the film diffusion is negligible and intraparticle diffusion is the only rate-controlling step, which is usually true for well-mixed solutions. An empirically found functional relationship, common to the most adsorption processes, is that the uptake varies almost proportionally with $t^{1/2}$, the Weber–Morris plot, rather than with the contact time t (Kavitha and Namasivayam 2007).

$$q_t = K_d t^{1/2} + C \tag{12}$$

where K_d is the intraparticle diffusion rate constant (g/(mg min$^{1/2}$)). According to Eq. (12), a plot of q_t versus $t^{1/2}$ should be a straight line with a slope K_d and intercept

C when adsorption mechanism follows the intraparticle diffusion process. Values of intercept give an idea about the thickness of boundary layer, i.e., larger the intercept with greater is the boundary layer effect.

In Fig. 5 plot of mass of Cr(VI) adsorbed per unit mass of adsorbent, q_t versus $t^{1/2}$ is presented for Cr(VI). The linear plots are attributed to the macro pore diffusion that is the accessible sites of adsorption. This is attributed to the instantaneous utilization of the most readily available adsorbing sites on the adsorbent surface (Kavitha and Namasivayam 2007). The values of K_d as obtained from the slope of straight lines was $0.0103 - 0.1265$ g/(mg min$^{1/2}$). As seen in Table 1, the correlation coefficient value R^2 for Cr(VI) adsorption onto the Fe(III)-impregnated sorbent changed in the range of $0.4281 - 0.9399$. These results have shown that the experimental data do not well agree with the intraparticle diffusion kinetic model.

Comparison of the applicability of different kinetic models

Among the four kinetic models, the pseudo-second-order equation generates the best fit to the experimental data of the three investigated adsorption systems at the initial Cr(VI) concentrations of 25, 50, and 100 mg/L for the entire adsorption period, with regression coefficients higher than $R^2 > 0.9946$ for the concentration range used in this study. The calculated q_e values from the model were also in good agreement with the experimental values. This indicates that the pseudo-second-order equation is potentially a generalized kinetic model for adsorption study. Kinetics of Cr(VI) adsorption onto the Fe(III)-impregnated sorbent followed the pseudo-second-order model, suggesting that the rate-limiting step may be chemisorption (Ho and McKay 1998). This confirmed that adsorption of Cr(VI) takes place probably via surface exchange reactions until the surface functional sites are fully occupied; thereafter chromate molecules diffuse into the adsorbent network for further interactions.

The other models generated a poor fit to the results of the experiments conducted for this study. For the pseudo-first-order kinetic model and the modified pseudo-first-order kinetic model, correlation coefficients were below 0.32 and the calculated q_e were not equal to experimental q_e, suggesting the insufficiency of the model to fit kinetic data for the initial concentrations examined. After a short period, the experimental data deviated considerably from linearity.

It is worth noting that the low correlation coefficients shown in Table 1 do not necessarily mean that the intraparticle diffusion process is not the rate-controlling step. It is a mere indication that the intraparticle diffusion model does not apply to the investigated adsorption systems (Yang and Al-Duri 2005). Actually, the plots of the amount of Cr(VI) adsorbed versus $t^{1/2}$ for intraparticle transport appeared to present a multilinearity which indicated that three steps occurred in the process (Fig. 5): (1) mass transfer across the external boundary layer film of liquid surrounding the outside of the particle, (2) adsorption at a site on the surface (internal or external) and the energy will depend on the binding process (physical or chemical); this step is often assumed to be extremely rapid, (3) diffusion of the adsorbate molecules to an adsorption site either by a pore diffusion process through the liquid filled pores or by a solid surface diffusion mechanism. The mechanism of adsorption is generally considered to involve three steps, one or any combination of which can be the rate-controlling mechanism (Yang et al. 2003). Thus, the intraparticle diffusion was not the only rate-limiting step, but other processes might control the rate of adsorption (Crini 2008; Doğan et al. 2007).

Adsorption isotherm

To optimize the design of an adsorption system for the adsorption of Cr(VI) onto Fe(III)-impregnated sorbent, it is important to establish the most appropriate correlation for the equilibrium curves. In this study, the equilibrium data of the adsorption of Cr(VI) onto the activated carbons prepared from sugarcane bagasse at of 20, 30, and 40°C were fitted with the Langmuir equation and the Freundlich equation.

Langmuir isotherm

Langmuir isotherm is represented by the following equation:

$$C_e/q_e = 1/(q_m \times K_L) + C_e/q_m \quad (13)$$

where C_e is the concentration of Cr(VI) solution (mg/L) at equilibrium. The constant q_m signifies the adsorption capacity (mg/g) and K_L is Langmuir constant related to the free energy of adsorption (L/mg). Linear plot of C_e/q_e versus C_e shows that adsorption follows Langmuir isotherm (Fig. 6). Values of q_m and K_L were calculated from the slope and intercept of the linear plot and are presented in Table 1.

The adsorption capacity can be correlated with the variation of surface area and porosity of the adsorbent. Higher surface area and pore volume will result in higher adsorption capacity (Kavitha and Namasivayam 2007).

The essential features of Langmuir adsorption isotherm can be expressed in terms of a dimensionless constant called the separation factor or equilibrium parameter (R_L), defined by Weber and Chakkravorti (Kavitha and Namasivayam 2007):

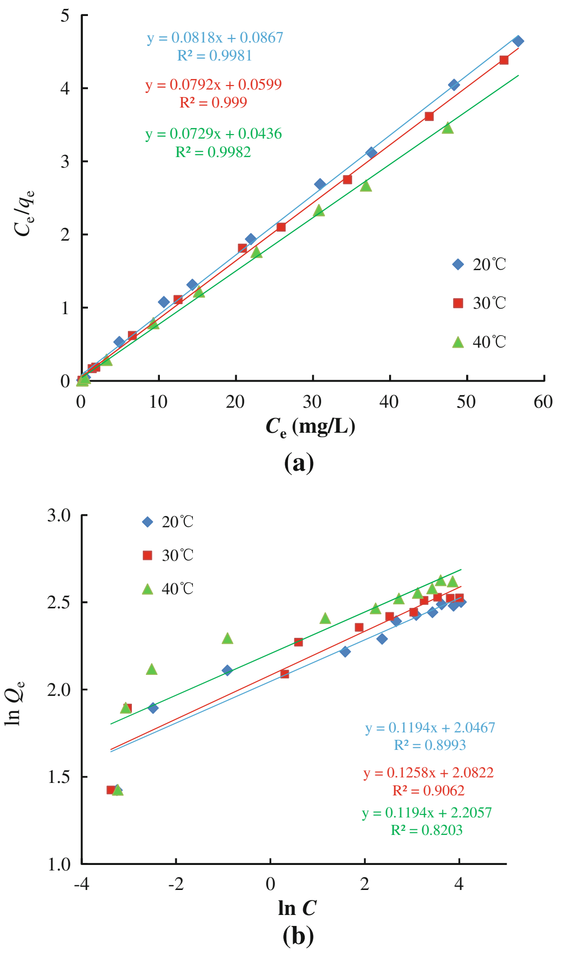

Fig. 6 Isotherm plots for Cr(VI) adsorption onto the Fe(III)-impregnated sorbent. **a** Langmuir isotherm, **b** Freundlich isotherm

$$R_L = 1/(1 + K_L C_0) \tag{14}$$

where K_L is the Langmuir adsorption constant and C_0 is the initial Cr(VI) concentration (mg/L).

The Langmuir equation is applicable to homogeneous adsorption, where the adsorption of each molecule onto the surface has equal adsorption activation energy (Crini 2008). The results of the fitting procedure are presented in Fig. 6 and Table 1, which show that the Langmuir isotherm could yield relatively poor fits over the whole concentration range for Cr(VI) adsorption onto the Fe(III)-impregnated sorbent, with R^2 values of 0.9981, 0.9990, and 0.9982 for the adsorption at 20, 30, and 40 °C, respectively. Conformation of the experimental data into Langmuir isotherm model with high R^2 value indicates the homogeneous nature of the adsorbent surface. Raising the temperature improved the adsorption capacity from 12.22 mg/g at 20 °C, 12.63 mg/g at 30 °C to 13.72 mg/g at 40 °C.

R_L values indicate the type of isotherms to be either unfavorable ($R_L > 1$), linear ($R_L = 1$), favorable ($0 < R_L < 1$), or irreversible ($R_L < 0$) (Crini 2008). Table 1 also shows R_L values near 0 confirmed the favorable uptake of the Cr(VI) process, which indicates favorable adsorption (Kavitha and Namasivayam 2007; Crini 2008).

Freundlich isotherm

The Freundlich isotherm can be used for non-ideal sorption that involves heterogeneous surface energy systems and is expressed by the following equation:

$$q_e = K_F C_e^{1/n} \tag{15}$$

where q_e refers to the amount of Cr(VI) adsorbed (mg/g) at equilibrium; C_e is the equilibrium concentration of Cr(VI) in solution (mg/L). Freundlich constant K_F ($\mathrm{mg}^{1-1/n}\mathrm{L}^{1/n}\mathrm{g}^{-1}$) is a rough indicator of the adsorption capacity and $1/n$ is the adsorption intensity.

In general, as the K_F value increases the adsorption capacity of an adsorbent for a given adsorbate increases. Eq. (15) may be linearised by taking logarithms:

$$\ln q_e = \ln K_F + 1/n \ln C_e \tag{16}$$

The values of K_F and n were calculated from intercept and slope of plots (Fig. 6, Table 1). The correlation coefficients (R^2) were found to be 0.8993, 0.9062, and 0.8203 for the adsorption at 20, 30, and 40 °C, respectively, and the Freundlich isotherm did not give a very good fit. $1/n$ is the heterogeneity factor and can be used as a measure of the deviation from linearity of the adsorption (Crini 2008). In this study, $1/n$ values were calculated from the slope of plots to be 0.1194 − 0.1258, which ranged between 0 and 1 and implied that adsorption process was chemical (Crini 2008).

Thermodynamic parameters

Increase of temperature increased the adsorption capacity. The change in free energy, enthalpy and entropy of adsorption were calculated from the experiments carried out at different temperatures using the following equations:

$$\Delta G^0 = -RT \ln K_L \tag{17}$$

where ΔG^0 is the standard free energy change, R is gas constant, K_L is the Langmuir constant and T is the temperature in Kelvin (K). According to van't Hoff equation,

$$\Delta G^0 = -RT \ln K_L = \Delta H^0 - T\Delta S^0 \tag{18}$$

The values of the standard enthalpy change (ΔH^0) and the standard entropy change (ΔS^0) were determined from the slope and the intercept of the linear plot of ΔG^0 versus T. As shown in Fig. 3, the adsorption capacity of Cr(VI) increased at higher temperatures, which indicated also that adsorption of Cr(VI) was an endothermic process. The negative values of the calculated ΔG^0 (−9.489, −10.663, and −11.626 kJ/mol) indicated the spontaneous nature of adsorption for Cr(VI) at 20, 30, and 40 °C and confirmed affinity of sorbent for Cr(VI). The positive calculated values of ΔH^0 (21.80 J/mol) showed the endothermic nature of adsorption. The positive values of ΔS^0 (0.1069 kJ/(mol K)) suggested the increased randomness at the solid/solution interface during the adsorption of Cr(VI) on the adsorbent (Wang and Zhu 2007).

Conclusion

With increasing initial Cr(VI) from 25 to 130 mg/L at an adsorbent dose of 300 mg/50 mL, the amount of Cr(VI) adsorbed on the Fe(III)-impregnated sorbent increased from 4.15–4.16 to 12.20–13.72 mg/g. The dynamical data fit very well with the pseudo-second-order kinetic model and the calculated adsorption capacities of 4.16, 8.37, and 13.37 mg/g were equal to the actual values of the experiments at the initial Cr(VI) of 25, 50, and 100 mg/L. The Langmuir isotherm could yield better fits than the Freundlich isotherm. The calculated isotherm parameters confirmed the favorable adsorption of Cr(VI) on the Fe(III)-impregnated sorbent.

Acknowledgments The manuscript has greatly benefited from insightful comments by two anonymous reviewers. The authors thank the Guangxi Key Laboratory of Environmental Engineering, Protection and Assessment for the research assistance and the financial support from the Provincial Natural Science Foundation of Guangxi, China (GuiKeZi 0832020Z, 2011GXNSFF018003, 2011GXNSFA018013).

References

Abdel-Ghani NT, Hegazy AK, El-Chaghaby GA (2009) Typha domingensis leaf powder for decontamination of aluminium, iron, zinc and lead: biosorption kinetics and equilibrium modeling. Int J Environ Sci Tech 6(2):243–248

Baçaoui A, Yaacoubi A, Dahbi A, Bennouna C, Phan Tan Luu R, Maldonado-Hodar FJ, Rivera-Utrilla J, Moreno-Castilla C (2001) Optimization of conditions for the preparation of activated carbons from olive-waste cakes. Carbon 39(3):425–432

Bayrak Y, Yesiloglu Y, Gecgel U (2006) Adsorption behavior of Cr(VI) on activated hazelnut shell ash and activated bentonite. Microporous Mesoporous Mater 91(1–3):107–110

Boussarsar H, Rogé B, Mathlouthi M (2009) Optimization of sugarcane bagasse conversion by hydrothermal treatment for the recovery of xylose. Bioresour Technol 100(24):6537–6542

Brandão PC, Souza TC, Ferreira CA, Hori CE, Romanielo LL (2010) Removal of petroleum hydrocarbons from aqueous solution using sugarcane bagasse as adsorbent. J Hazard Mater 175(1–3): 1106–1112

Chu KH, Hashim MA (2002) Adsorption characteristics of trivalent chromium on palm oil fuel ash. Clean Technol Environ Policy 4(1):8–15

Crini G (2005) Recent developments in polysaccharide-based materials used as adsorbents in wastewater treatment. Prog Polym Sci 30(1):38–70

Crini G (2008) Kinetic, equilibrium studies on the removal of cationic dyes from aqueous solution by adsorption onto a cyclodextrin polymer. Dye Pigment 77(2):415–426

Doğan M, Özdemir Y, Alkan M (2007) Adsorption kinetics and mechanism of cationic methyl methylene blue dyes onto sepiolite. Dye Pigment 75(3):701–713

Gupta S, Babu BV (2009) Removal of toxic metal Cr(VI) from aqueous solutions using sawdust as adsorbent: Equilibrium, kinetics and regeneration studies. Chem Eng J 150(2–3):352–365

Ho YS, McKay G (1998) Kinetic models for the sorption of dye from aqueous solution by wood. Process Saf Environ 76(2):183–191

Ioannidou O, Zabaniotou A (2007) Agricultural residues as precursors for activated carbon production - A review. Renew Sust Energ Rev 11(9):1966–2005

Kavitha D, Namasivayam C (2007) Experimental and kinetic studies on methylene blue adsorption by coir pith carbon. Bioresour Technol 98(1):14–21

Khalili NR, Campbell M, Sandi G, Golaś J (2000) Production of micro- and mesoporous activated carbon from paper mill sludge: I. Effect of zinc chloride activation. Carbon 38(14):1905–1915

McKay G, Ho YS (1999) Pseudo-second order model for sorption processes. Process Biochem 34(5):451–465

Mohan D, Pittman CU Jr (2006) Activated carbons and low cost adsorbents for remediation of tri- and hexavalent chromium from water. J Hazard Mater 137(2):762–811

Mohan D, Singh KP (2002) Single- and multi-component adsorption of cadmium and zinc using activated carbon derived from bagasse: an agricultural waste. Water Res 36(9):2304–2318

Okoye AI, Ejikeme PM, Onukwuli OD (2010) Lead removal from wastewater using fluted pumpkin seed shell activated carbon: Adsorption modeling and kinetics. Int J Environ Sci Tech 7(4):793–800

Qureshi K, Bhatti I, Kazi R, Ansari AK (2008) Physical and chemical analysis of activated carbon prepared from sugarcane bagasse and use for sugar decolorisation. Int J Chem Biol Eng 1–3: 145–149

Rafati L, Mahvi AH, Asgari AR, Hosseini SS (2010) Removal of chromium (VI) from aqueous solutions using Lewatit FO36 nano ion exchange resin. Int J Environ Sci Tech 7(1):147–156

Sahu JN, Acharya J, Meikap BC (2010) Optimization of production conditions for activated carbons from Tamarind wood by zinc chloride using response surface methodology. Bioresour Technol 101:1974–1982

Samani MR, Borghei SM, Olad A, Chaichi MJ (2010) Removal of chromium from aqueous solution using polyaniline–poly ethylene glycol composite. J Hazard Mater 184(1–3):248–254

Wang S, Zhu ZH (2007) Effects of acidic treatment of activated carbons on dye adsorption. Dyes Pigments 75(2):306–314

Witek-Krowiak A, Szafran RG, Modelski S (2010) Biosorption of heavy metals from aqueous solutions onto peanut shell as a low-cost biosorbent. Desalination 265(1–3):126–134

Wong SY, Tan YP, Abdullah AH, Ong ST (2009) The removal of basic and reactive dyes using quartenised sugarcane bagasse. J Phys Sci 20(1):59–74

Yang XY, Al-Duri B (2005) Kinetic modeling of liquid-phase adsorption of reactive dyes on activated carbon. J Colloid Interf Sci 287(1):25–34

Yang XY, Otto SR, Al-Duri B (2003) Concentration-dependent surface diffusivity model (CDSDM): numerical development and application. Chem Eng J 94(3):199–209